© 2002 WIT Press, Ashurst Lodge, Southampton, SO40 7AA, UK. All rights reserved.
Web: www.witpress.com Email witpress@witpress.com
Paper from: *Structures Under Shock and Impact VII*, N Jones, CA Brebbia and AM Rajendran (Editors).
ISBN 1-85312-911-9

Modelling of concrete perforation

H. Hansson
Weapons and Protection,
Swedish Defence Research Agency (FOI), Sweden

Abstract

This paper describes work done with the RHT concrete model developed at EMI, which shows promising behaviour for penetration/perforation simulations in concrete. The results from a benchmark test series from 1999 with 152 mm ogive nosed projectiles are briefly described and also used as a reference case for the simulations. The tests were a co-operation project with DERA (now DSTL), FFI, FOA (now FOI) and TNO as participants. Numerical simulations with Lagrange, Euler and SPH formulations are compared with the benchmark tests, and the strengths as well as weaknesses of the different formulations are discussed.

1 Introduction

It is necessary to predict penetration depths in concrete targets to determine the vulnerability of underground structures. Several empirical and numerical tools are developed to predict penetration depths of projectiles in concrete. An advanced material model is used to describe the material behaviour of concrete in this study. The material model is then combined with Euler and SPH numerical formulations to study projectile penetration in concrete targets. Numerical simulations with the Lagrange formulation and earlier performed benchmark tests are used for comparison with the performed Euler and SPH simulations.

2 The RHT concrete model

The RHT material model is implemented in the general release of Autodyn 4.2 and the model is presented by Riedel [1]. However, a few modifications to the material model were made before the implementation in Autodyn. Earlier simulations with the material model are presented by Riedel et al [2], and

© 2002 WIT Press, Ashurst Lodge, Southampton, SO40 7AA, UK. All rights reserved.
Web: www.witpress.com Email witpress@witpress.com
Paper from: *Structures Under Shock and Impact VII*, N Jones, CA Brebbia and AM Rajendran (Editors).
ISBN 1-85312-911-9

Hansson and Ågårdh [3]. Svinsås et al [4] have presented simulations of the benchmark tests with the RHT model as a user routine implemented for Autodyn 2D version 4.1.13 by EMI.

The material model uses three strength surfaces, these are an elastic limit surface, failure surface and remaining strength surface for the crushed material. There is also an option to use a cap on the elastic strength surface. In figure 1 the elastic strength surface with cap and the failure surface are shown. The pressure dependence of the failure strength is given on a normalised form according to eqn (1) with p_{spall} defined as the failure pressure under hydrostatic expansion. The reduction of the failure strength between the compression and the tension meridians is given by eqn (2) and (3). The model also accounts for the loading rate according to eqn (4). There is also an option in the model to use a cap on the elastic strength surface. The various effects are given as factors according to eqn (5), where $f = 0$ defines points on the failure surface.

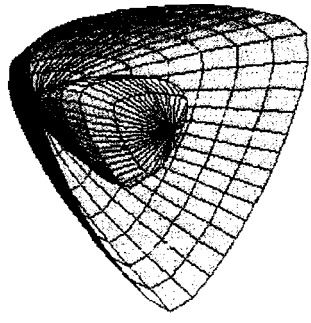


Figure 1: Elastic strength surface with cap and failure surface for the RHT model, from Riedel [1].

$$Y^*_{TXC(P)} = \frac{Y_{TXC(p)}}{f'_c} = A_{fail} \cdot \left[p^* - \left(p^*_{spall} F_{Rate}\right)\right]^{N_{fail}}. \tag{1}$$

$$R_3(\theta) = \frac{2\left(1-Q_2^2\right)\cos\theta + \left(2Q_2 - 1\right)\left[4\left(1-Q_2^2\right)\cos^2\theta + 5Q_2^2 - 4Q_2\right]^{\frac{1}{2}}}{4\left(1-Q_2^2\right)\cos^2\theta + \left(1-2Q_2\right)^2}. \tag{2}$$

$$Q_2 = Q_{2,o} + BQ \cdot p^* \text{ with } 0.5 \le Q_2 \le 1 \text{ and } BQ = 0.0105. \tag{3}$$

$$F_{RATE(\dot{\varepsilon})} = \begin{cases} \left(\dfrac{\dot{\varepsilon}}{\dot{\varepsilon}_0}\right)^{\alpha} & \text{for } P > f_c/3 \text{, with } \dot{\varepsilon}_0 = 30\times10^{-6}\ s^{-1}. \\ \left(\dfrac{\dot{\varepsilon}}{\dot{\varepsilon}_0}\right)^{\delta} & \text{for } P < f_c/3 \text{, with } \dot{\varepsilon}_0 = 3\times10^{-6}\ s^{-1}. \end{cases} \tag{4}$$

$$f(p, \sigma_{eq}, \theta, \dot{\varepsilon}) = \sigma_{eq} - Y_{TXC(P)} F_{CAP(P)} R_{3(\theta)} F_{RATE\ (\dot{\varepsilon})}. \tag{5}$$

© 2002 WIT Press, Ashurst Lodge, Southampton, SO40 7AA, UK. All rights reserved.
Web: www.witpress.com Email witpress@witpress.com
Paper from: *Structures Under Shock and Impact VII*, N Jones, CA Brebbia and AM Rajendran (Editors).
ISBN 1-85312-911-9

The damage in the material grows after the stress point passes the failure surface according to eqn (6). The strength is interpolated from the strength values for the undamaged material (D=0) and the completely damaged material (D=1) according to eqn (7), depending on the accumulated damage. More parameters that define the strength surfaces and damage are given in table 1.

$$D = \sum \frac{\Delta \varepsilon_p}{\varepsilon_p^{failure}} \quad with \quad \varepsilon_p^{failure} = D_1 \left(P^* - P^*_{spall} \right)^{D_2} . \tag{6}$$

$$Y^*_{fractured} = (1-D) Y^*_{failure} + D \cdot Y^*_{residual} \quad with \quad Y^*_{residual} = B \cdot \left(P^* \right)^M . \tag{7}$$

Table 1: Parameter definitions for the RHT concrete model, see also the equations above.

Parameter	Description
f_c	Compressive strength
A_{fail}	Constant for pressure dependence of failure strength
N_{fail}	Exponent for pressure dependence of failure strength
f_t/f_c	Tensile compressive strength ratio
f_s/f_c	Shear compressive strength ratio
Q_2	Tensile compression meridian ratio
BQ	Brittle to ductile transition
$\frac{G_{elastic}}{G_{elastic-plastic}}$	Ratio between elastic shear modulus and elastic-plastic shear modulus. (PREFACT)
$f_{t,\,elastic}/f_t$	Ratio between elastic surface and failure surface for tension (TENSRAT)
$f_{c,\,elastic}/f_c$	Ratio between elastic surface and failure surface for compression (COMPRAT)
B	Constant for pressure dependence of residual strength
M	Exponent for pressure dependence of residual strength
$\varepsilon_{fail,\,min}$	Minimum strain to failure
$G_{residual}/G_{elastic}$	Residual shear modulus fraction (SHRATD)
ν	Specific volume
α	ν_{porous}/ν_{solid} for EOS, and compressive strain rate exponent for F_{RATE}

The equation of state is based on the P-α model presented by Herrmann [5]. The behaviour of the solid material is given by eqn (8a-b), while the porous compaction is given by eqn (9). The pressure as function of density and energy (e) gives the behaviour of the porous material in the pressure range of pore collapse (p_{crush}) and full compaction (p_{look}) for α=1. The pressure for the porous material is approximate $1/\alpha$ times the pressure in the matrix material. Therefore the use of this correction term in eqn (9).

© 2002 WIT Press, Ashurst Lodge, Southampton, SO40 7AA, UK. All rights reserved.
Web: www.witpress.com Email witpress@witpress.com
Paper from: *Structures Under Shock and Impact VII*, N Jones, CA Brebbia and AM Rajendran (Editors).
ISBN 1-85312-911-9

$$p = A_1\mu + A_2\mu^2 + A_3\mu^3 \quad with \quad \mu = \frac{\rho}{\rho_0} - 1 \geq 0 . \tag{8a}$$

$$p = T_1\mu + T_2\mu^2 \quad with \quad \mu = \frac{\rho}{\rho_0} - 1 < 0 . \tag{8b}$$

$$p = f(\rho_{solid}, e) \overset{porous}{\rightarrow} p = \left(\frac{1}{\alpha}\right) \cdot f(\rho \cdot \alpha, e)$$

$$with\ \alpha = 1 + (\alpha_{initial} - 1)\left[\frac{p_{lock} - p}{p_{lock} - p_{crush}}\right]^n . \tag{9}$$

3 Benchmark tests

A benchmark test series with 152 mm projectiles was conducted in 1999. The aim of the test was to obtain data for comparison with numerical simulation.

3.1 Material properties

The concrete for the benchmark test series was tested with standard methods to obtain E-modulus, cube strength and splitting strength. The behaviour of the concrete during tri-axial loading was tested with passive confinement of the concrete with GREAC cells by FFI and Imperial College. The properties of concrete/targets are given in table 2 and figure 2. See also figure 5 for the relationship between pressure and density for the concrete. Further data are given by Hansson [6].

Table 2: Properties of the concrete targets.

Target/concrete properties	Value
Diameter	2.40 m
Length	0.75 m
f_c , ∅100×200 mm cylinders	92 ± 2 MPa
Tensile splitting strength, 150 mm cubes	6.5 ± 0.2 MPa
E_c for ∅100×200 mm cylinders	44.5 ± 0.9 GPa

© 2002 WIT Press, Ashurst Lodge, Southampton, SO40 7AA, UK. All rights reserved.
Web: www.witpress.com Email witpress@witpress.com
Paper from: *Structures Under Shock and Impact VII*, N Jones, CA Brebbia and AM Rajendran (Editors).
ISBN 1-85312-911-9

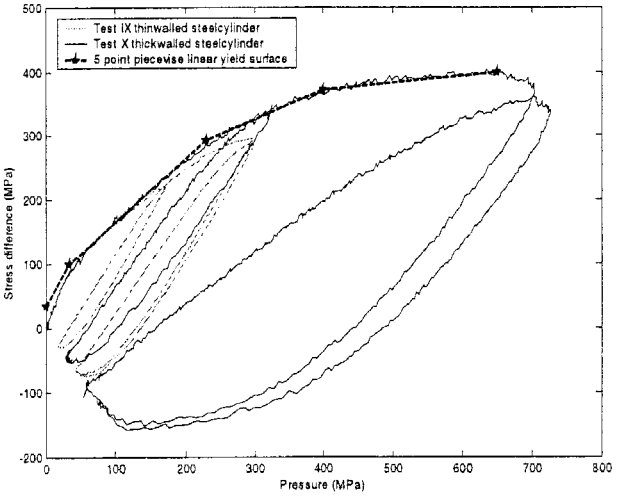


Figure 2: The measured difference between axial and radial stresses vs. pressure for concrete samples tested in a GREAC cell at FFI.

3.2 Perforation tests

Three benchmark tests were performed with a 152 mm projectile, see figure 3 and table 3. A Doppler radar was used to determine impact velocity and the velocity of the projectile during the first phase of the penetration, and this radar measurements seem to have registered the velocity during the major part of the projectile deceleration in the target. The exit velocity of the projectiles was determined with a high speed video camera. A target after perforation is shown in figure 4. Further data are given by Hansson [6].

Table 3: Benchmark test data.

Test	No. 23	No. 24	No. 25	Mean value
Projectile properties	Diameter 152 mm, length 552 mm, ogive radius 380 mm, total mass 46.2 ±0.1 kg, case mass 38.8 kg			
V_{Impact} (m/s)	460.0 ±0.5	455.5 ±0.2	458.8 ±0.2	458.1 ±0. 2
V_{Exit} (m/s)	183 ±6	204 ±4	181 ±4	190 ±14



Figure 3: 152 mm projectile used for tests.

© 2002 WIT Press, Ashurst Lodge, Southampton, SO40 7AA, UK. All rights reserved.
Web: www.witpress.com Email witpress@witpress.com
Paper from: *Structures Under Shock and Impact VII*, N Jones, CA Brebbia and AM Rajendran (Editors).
ISBN 1-85312-911-9

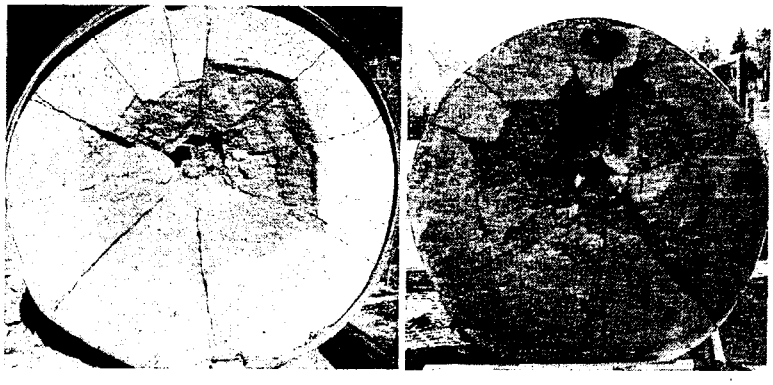


Figure 4: Target after perforation for test no. 24, front face to the left.

4 Numerical simulation of benchmark tests

The simulations of concrete perforation were performed with Autodyn 2D version 4.2.00v (β-release). Initial numerical simulations were also performed to study the behaviour of the RHT concrete model. Numerical simulations of the benchmark tests are also presented by Svinsås et al [4].

4.1 Material parameters used for simulation with the RHT model

The chosen values of the material parameters for the RHT model were based on the material test described in the previous chapter. The tensile strength was chosen as 5.2 MPa, this is approximate 80% of the splitting strength for 150 mm cubes. The initial bulk and shear moduli were based on the measured initial Young's modulus and a Poisson's ratio of 0.18. The strain rate enhancement for the concrete is based on comparison with similar concrete types. The hydro tensile limit was used as tensile failure condition for the simulations. Used values for the material parameters are given in tables 4, and 6 to 9. Hansson [6] has presented further data from the simulations.

Table 4: Common parameters for simulations with the RHT concrete model.

Parameter	Value	Parameter	Value
G	18 GPa	PREFACT	2
f_c	92 MPa	TENSRAT	0.80
f_t/f_c	0.057	COMPRAT	0.75
f_s/f_c	0.30	Cap on elastic surface	Yes
A_{fail}	1.9	B	1.6
N_{fail}	0.6	M	0.61
Q_2	0.6805	α (for F_{RATE})	0.010
BQ	0.0105	δ	0.013
		SHRATD	0.13

© 2002 WIT Press, Ashurst Lodge, Southampton, SO40 7AA, UK. All rights reserved.
Web: www.witpress.com Email witpress@witpress.com
Paper from: *Structures Under Shock and Impact VII*, N Jones, CA Brebbia and AM Rajendran (Editors).
ISBN 1-85312-911-9

The behaviour of the material model was tested for hydrostatic pressure loading, with the obtained pressure vs. density relationship shown in figure 5. Uni-axial compressive stress was also simulated to determine the model's response at different loading rates. The calculated relationship between deformation and uni-axial stress is given in figure 6 where the dependence of strain rate from 0.1 to 10 s^{-1} is shown.

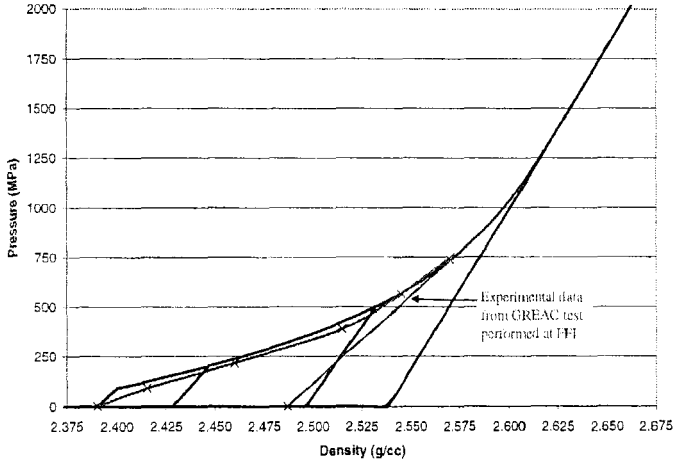


Figure 5: Hydrostatic loading and unloading path for the concrete.

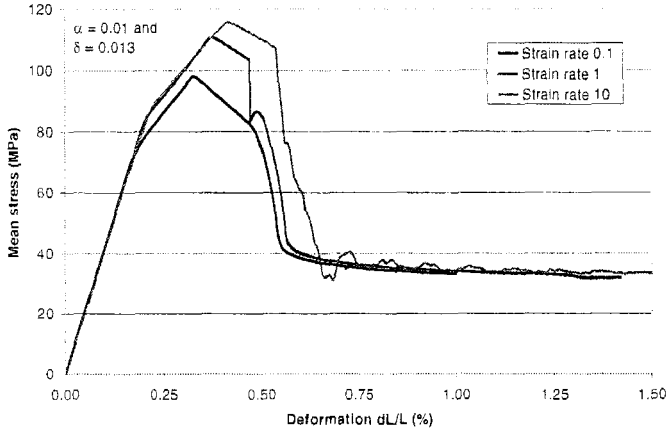


Figure 6: Uni-axial compressive stress vs. axial deformation for different strain rates.

© 2002 WIT Press, Ashurst Lodge, Southampton, SO40 7AA, UK. All rights reserved.
Web: www.witpress.com Email witpress@witpress.com
Paper from: *Structures Under Shock and Impact VII*, N Jones, CA Brebbia and AM Rajendran (Editors).
ISBN 1-85312-911-9

4.2 Numerical simulation of penetration with the RHT model

The numerical simulations of the benchmark test were performed with Lagrange, Euler and SPH formulation for comparison, see table 5. For the Lagrange formulation it is necessary to use numerical erosion. However, this reduces the confinement in the models. Concrete has a pressure dependent yield stress and failure type, and the calculation results are therefore likely to be influenced by the use of numerical erosion. The Euler and SPH formulations do not require the use of numerical erosion. All models for the penetration simulations used 2D axial symmetry with the geometry shown in figure 7. Further data on the simulations are given by Hansson [6] and Hansson et al [7].

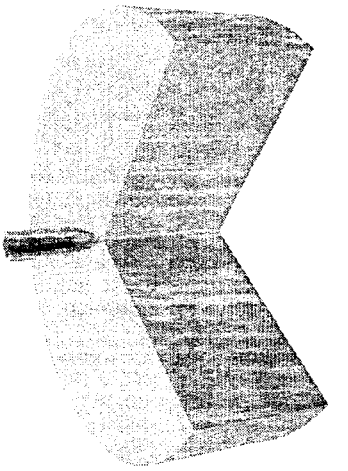


Figure 7: The geometry for the simulations is shown with 270° rotation of the 2D model for visualisation.

Table 5: Model properties for the different numerical formulations.

Target formulation	Lagrange	Euler	SPH
Element size in target	10×10 mm or 5×5 mm		5 mm nodes
Elements for projectile	15×10 mm Lagrange elements		
Projectile mass	46.2 kg		
Projectile velocity	459 m/s		
Erosion strain	150%	No erosion	

The friction between target and projectile was varied for the Lagrange and SPH models. However, the use of friction for Lagrange models is likely to increase the shear strain in the target, and thereby distort the elements to a higher degree. A limited study of the influence from the damage parameters (D_1, D_2, EFMIN) was conducted. These parameters are together with the residual strength parameters (B, M) of the concrete among those that are likely to greatly influence the exit

© 2002 WIT Press, Ashurst Lodge, Southampton, SO40 7AA, UK. All rights reserved.
Web: www.witpress.com Email witpress@witpress.com
Paper from: *Structures Under Shock and Impact VII*, N Jones, CA Brebbia and AM Rajendran (Editors)
ISBN 1-85312-911-9

velocity of the projectile, see Hansson [6]. The influence from the size of the elements in the model was checked with simulations with 5 mm Lagrange elements. This model offers less resistance for the projectile compared to the model with 10 mm element size and the same model properties. This is likely to be caused by the numerical erosion in the model, and the erosion strain should therefore be increased when the element size is decreased. Some results from the Lagrange simulations are shown in tables 6 and 7.

The exit velocities for the simulations B99036 and B99057 have a good agreement with the experimental results. If these model parameters also result in an acceptable accuracy for other similar experiments need to be evaluated in the future. In figure 8 the measured velocity from the radar are compared with the calculated velocity for model B99057.

Table 6: Lagrange models with 10 mm element size with variation of damage parameters.

Model	B99008	B99036	B99038
Element size	10×10 mm		
D_1	0.04	0.08	0.04
EFMIN	0.01	0.05	
Friction coefficient	No friction		
Exit velocity	247 m/s	189 m/s	212 m/s
Energy error	0.9 %	1.0 %	1.1 %

Table 7: Lagrange models with 5 mm element size, and different damage parameters.

Model	B99055	B99056	B99057
Element size	5×5 mm		
D_1	0.04	0.08	
EFMIN	0.01	0.05	
Friction coefficient	No friction		0.05
Exit velocity	269 m/s	237 m/s	207 m/s
Energy error	0.5 %	0.6 %	8.6 %

© 2002 WIT Press, Ashurst Lodge, Southampton, SO40 7AA, UK. All rights reserved.
Web: www.witpress.com Email witpress@witpress.com
Paper from: *Structures Under Shock and Impact VII*, N Jones, CA Brebbia and AM Rajendran (Editors).
ISBN 1-85312-911-9

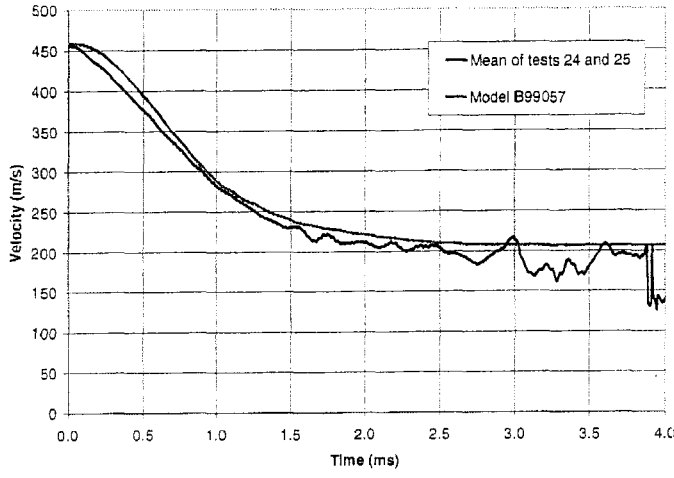


Figure 8: Comparison between calculated velocity for model B99057 and data from radar measurement.

The use of an Eulerian target formulation has one major advantage compared with a Lagrangian formulation, and that is the fixed element mesh. Instead of deforming the elements with the material, the material is transported between fixed elements for the Euler formulation. The Euler models have generally an increased exit velocity when compared to the Lagrange models with the same material properties. This might be due to the transportation algorithms and the difficulties to track the status of material during the simulation. The parameters for the calculated Euler simulations are compiled in table 8.

Table 8: Euler models of benchmark tests.

Model	B99E03	B99E05	B99E55
Element size	10×10 mm		5×5 mm
D_1	0.04	0.08	
EFMIN	0.01	0.05	
Friction	No friction		
Exit velocity	265 m/s	246 m/s	255 m/s
Energy error	0.2 %	0.3 %	0.1 %

Numerical simulations of the benchmark tests were also performed with SPH formulation, these are presented by Hansson et al [7]. The properties for the SPH models are given in table 9. The SPH model shows a greater penetration resistance than obtained both for the Euler and Lagrange simulations with the same material parameters. This is likely to be an effect of the earlier discussed numerical problems for Lagrange and Euler formulations. Damage plots for Lagrange, Euler and SPH simulations are shown in figure 9.

© 2002 WIT Press, Ashurst Lodge, Southampton, SO40 7AA, UK. All rights reserved.
Web: www.witpress.com Email witpress@witpress.com
Paper from: *Structures Under Shock and Impact VII*, N Jones, CA Brebbia and AM Rajendran (Editors).
ISBN 1-85312-911-9

Table 9: Models with 5 mm SPH nodes of benchmark tests.

Model	B99S00	B99S01
Element size in target	5 mm SPH nodes	
EFMIN	0.05	
D2	0.08	
Friction coefficient	0	0.05
Exit velocity	214 m/s	186 m/s
Energy error	0.5 %	9.2 %

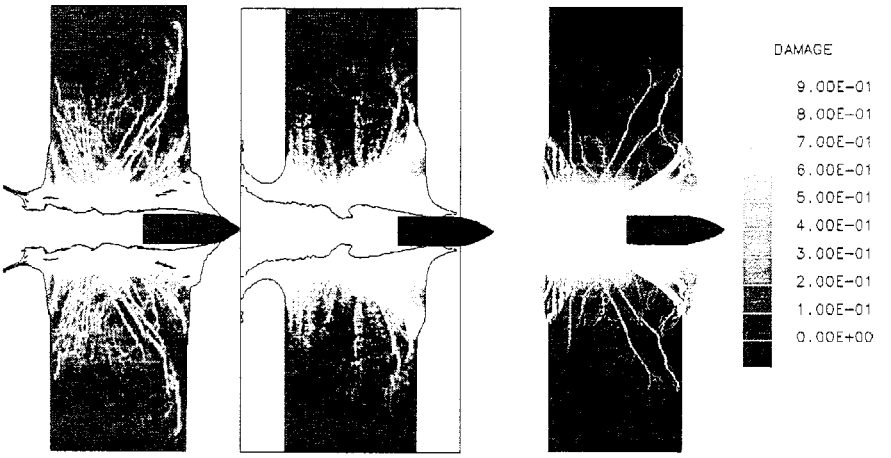


Figure 9: Damage plots from left for models B99056 with Lagrange elements, B99E55 with Euler elements and B99S00 with SPH nodes. All models with 5 mm elements/nodes and without friction.

5 Discussion

For the simulations performed with the Lagrange element formulation it is necessary to use numerical erosion to obtain a solution by deleting distorted elements. Because of this, the mass and confinement in the model decreases during the calculation. This has a large influence on the simulation results, at least when advanced material models with pressure dependent yield and/or failure is used. Therefore, numerical erosion should be avoided. This can be done with the use of Eulerian or SPH formulation. With the latest development in material and numerical modelling it is possible to use alternative element formulation in combination with advanced material models. Autodyn can i.e. use the RHT concrete model combined with Lagrange, ALE, Euler and SPH formulation.

Simulations with Eulerian and SPH formulation for the concrete targets, and the use of the RHT concrete model have shown promising results. Both the Euler and SPH formulations make it possible to retain the material of the target during

© 2002 WIT Press, Ashurst Lodge, Southampton, SO40 7AA, UK. All rights reserved.
Web: www.witpress.com Email witpress@witpress.com
Paper from: *Structures Under Shock and Impact VII*, N Jones, CA Brebbia and AM Rajendran (Editors).
ISBN 1-85312-911-9

the simulation. With these methods it is possible to start to identify problems regarding the material descriptions. For the simulations performed with Lagrangian element formulation it is very difficult to distinguish between errors caused by numerical problems, i.e. from distorted elements and erosion, and errors caused by the material models.

Parameters that influence the calculation result greatly are the residual strength of the failed concrete and the parameters for damage evolution. Because of this it is necessary to develop testing methods to determine damage development in the concrete and strength of damaged or partly damaged concrete.

References

[1] Riedel, W., *Beton unter dynamishen lasten, Meso- und makromechanische modelle und ihre parameter*. EMI-Bericht 6/00, EMI Freiburg, 2000.

[2] Riedel, W., Thoma K, Hiermaier S, Schmolinske E, Penetration of Reinforced Concrete by BETA-B-500. Numerical Analysis using a New Macroscopic Concrete Model for Hydrocodes. *Proc.of 9th Int. Symp. on Interaction of the Effects of Munitions with Structures*, pp. 315-322, 1999.

[3] Hansson, H. and Ågårdh, L., Experimental and numerical studies of projectile perforation in concrete targets. *Proc. Structural failure and plasticity symp. (IMPLAST 2000)*, Elsevier: Oxford, pp. 115-120, 2000.

[4] Svinsås, E., O'Carroll, C., Wentzel, C. M. and Carlberg' A., Benchmark trial designed to provide validation data for modelling. *Proc. of 10th Int. Symp. on Interaction of the Effects of Munitions with Structures*. 2001.

[5] Herrmann, W., Constitutive Equation for the Dynamic Compaction of Ductile Porous Materials. *Journal of App Physics*, Vol 40, No 6, pp. 2490-2499, 1969.

[6] Hansson, H., *Numerical simulation of concrete penetration with Euler and Lagrange formulations*. FOI-R--0190--SE, FOI Tumba, 2001.

[7] Hansson, H., Skoglund, P. and Unosson, M., *Structural protection for tactical stationary/mobile behaviour 2001*. FOI-R--0281--SE, FOI Tumba, 2001.